STRUCTURE OF TURBULENT CHANNEL FLOW WITH SQUARE BARS ON ONE WALL

S. Leonardi, P. Orlandi
Dipartimento di Meccanica e Aeronautica, University of Rome "La Sapienza", 00184, Rome, Italy

L. Djenidi & R. A. Antonia
Discipline of Mechanical Engineering, University of Newcastle, NSW 2308 Australia

ABSTRACT

The organised motion in a turbulent channel flow with a succession of square bars on the bottom wall has been investigated using direct numerical simulations. Four values (1,3,7,19) of the ratio w/k, where k is the bar height and w is the longitudinal separation between consecutive bars have been examined in detail. Relative to a smooth surface, the streamwise extent of the near-wall structures is decreased while their spanwise extent is increased. As w/k increases, the coherence decreases in the streamwise direction and increases in the spanwise direction. Reynolds stresses and their anisotropy invariants show a closer approach to isotropy over the rough wall than over a smooth wall.

INTRODUCTION

Since the pioneering work of Kline *et al.* (1967), a wealth of information is now available on the structure of a turbulent boundary layer on a smooth wall (e.g. Cantwell 1981; Robinson 1991). Much less is known on a turbulent boundary layer over rough surfaces. In particular, the effect the roughness has on the near-wall structure of the boundary layer is far from complete. Arguably, this state of affairs relates to the difficulties of carrying out reliable measurements in the vicinity of the roughness. Further, the number of parameters that affect the flow, (for example the density, height, shape of the roughness as well as its nature, e.g. 2D or 3D) compounds these difficulties. Despite these problems, useful results have emerged from experimental studies of boundary layers over rough walls. Several previous studies have considered how the low-speed streaks are influenced by roughness. The flow visualizations of Grass *et al.*(1967) over a rough wall made up of spheres indicated that the distance between the streaks increased, whereas their streamwise coherence was reduced relative to a smooth wall. Consistently, Krogstad and Antonia (1994) found that two-point correlations over a mesh roughness indicated a decrease in streamwise correlation with a slight increase in the spanwise extent of the structures. Different features are observed over a particular (so-called "d-type") rough wall made of square bars attached to the wall transversely to the flow,the streamwise distance between consecutive bars being equal to the bar height (e.g. Perry *et al.* 1969; Wood and Antonia 1975; Djenidi *et al.* 1999). For a d-type roughness, the latter authors found low and high-speed streaks alternating in the spanwise direction with approximately the same normalised spacing as over a flat wall.

A systematic study of the changes caused by varying w/k has yet to be attempted in experiments. Here, we address this in some detail, by analysing numerical results obtained at four values of w/k. In particular, we consider two-point velocity correlations, with the fixed point at several locations within one roughness wavelength. We also consider the effect w/k has on the way the cavity communicates with the overlying flow. The departure from isotropy of the Reynolds stress tensor is also examined in the context of its anisotropy invariants.

NUMERICAL PROCEDURE

The non-dimensional Navier-Stokes and continuity equations for incompressible flows are:

$$\frac{\partial U_i}{\partial t}+\frac{\partial U_i U_j}{\partial x_j}=-\frac{\partial P}{\partial x_i}+\frac{1}{Re}\frac{\partial^2 U_i}{\partial x_j^2}+\Pi\,, \qquad \nabla\cdot U=0 \quad (1)$$

where $Re = (U_c h/\nu)$ is the Reynolds number, h is the channel half-width, U_c is the centreline velocity, ν is the kinematic viscosity, Π is the pressure gradient required to maintain a constant flow rate, U_i is the component of the velocity vector in the i direction and P is the pressure. The Navier-Stokes equations have been discretized in an orthogonal coordinate system using the staggered central second-order finite-difference approximation. Here, only the main features are recalled since details of the numerical method can be found in Orlandi (2000). The discretized system is advanced in time using a fractional-step method with viscous terms treated implicitly and convective terms explicitly. The large sparse matrix resulting from the implicit terms is inverted by an approximate factorisation technique. At each time step, the momentum equations are advanced with the pressure at the previous step, yielding an intermediate non-solenoidal velocity field. A scalar quantity Φ projects the non-solenoidal field onto a solenoidal one. A hybrid low-storage third-order Runge-Kutta scheme is used to advance the equations in time. The roughness is treated by the efficient immersed boundary technique described in detail by Fadlun *et al.* (2000). This approach allows the solution of flows over complex geometries without the need of computationally intensive body-fitted grids. It consists of imposing $U_i = 0$ on the body surface which does not necessarily coincide with the grid. Another condition is required to avoid that the geometry is described in a stepwise way. Fadlun *et al.* (2000) showed that second-order accuracy is achieved by evaluating the velocities at the closest point to the boundary using a linear interpolation. This is consistent with the presence of a linear mean velocity profile very near the boundary even for turbulent flows, albeit at the expense of clustering more points near the body.

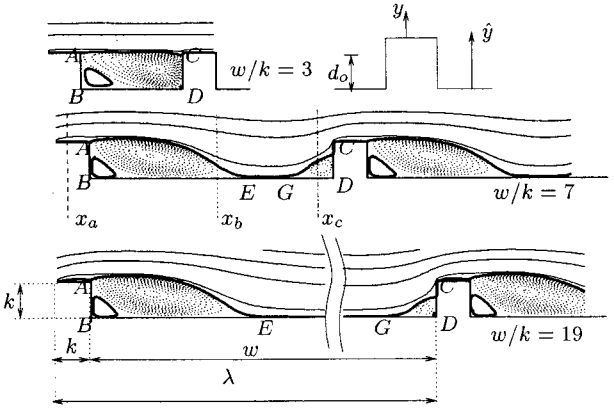

Figure 1: Mean streamlines, averaged with respect to time and z, for different w/k. The thick line corresponds to the zero streamfunction. ——— positive streamfunction, - - - - negative (primary recirculation zone). The definitions of $k, w, d_o, y, \hat{y}, x_a, x_b, x_c$ and λ are indicated. Flow is left to right.

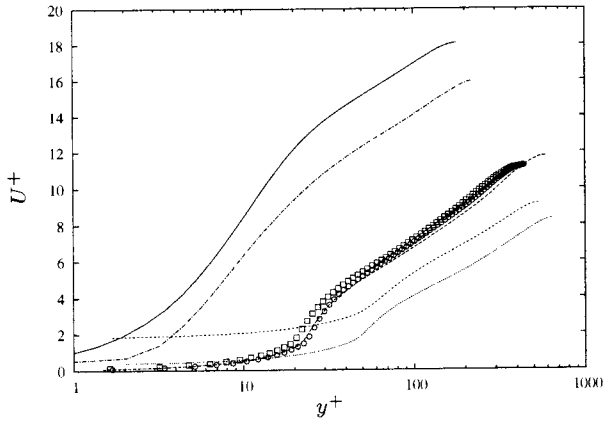

Figure 2: Velocity profiles in wall units, averaged in time and spanwise direction. ——— Kim & Moin (1987), —·— $w/k = 1$, ····· $w/k = 7$, - - - - $w/k = 19$. $w/k = 3$, $Re = 4200$ □ large channel, ○ narrow channel, - - - - $Re = 6000$ large channel.

FLOW CONFIGURATION

Direct numerical simulations have been performed for a fully developed turbulent channel flow with square bars on the bottom wall. Four values (1,3,7,19) of w/k within of the larger database (0.33, 0.6, 1, 2.07, 3, 4, 5.5, 7, 8, 9, 10, 19) carried out by the authors (see Leonardi 2002), have been investigated in more detail, with particular emphasis on the correlations. Periodic boundary conditions apply in the streamwise (x) and spanwise (z) directions respectively, and a no slip condition at the wall. The computational box is $8h \times 2h \times 4h$ in x, y (wall–normal direction) and z respectively (figure 1), the roughness height is $k = 0.2h$.

The Reynolds number is $Re = 4200$ and corresponds to $h^+ = 180$ when both walls are smooth. The superscript "+" denotes normalisation by either U_τ ($\equiv (\tau/\rho)^{1/2}$), τ is the wall shear stress equal to the sum of the skin frictional drag and form drag) or ν/U_τ. The flow rate has been kept constant in all simulations, hence U_τ, k^+ and h^+ depend on w/k. Three different grids have been used for all the simulations, $200 \times 140 \times 97$, $400 \times 140 \times 97$ and $300 \times 140 \times 97$. The first two are non-uniform in y while the third is non-uniform in x and y. In the normal direction, the points are clustered near the wall (within the cavity $\Delta y|_{min}/h$ is 0.005). The mesh increases up to $\Delta y|_{max}/h = 0.03$ at the channel centreline. In x, points are clustered near the roughness elements. Results obtained with the $300 \times 140 \times 97$ and $400 \times 140 \times 97$ grids are virtually identical. Only results obtained with the latter grid are given here.

For $w/k = 3$(with $k = .2h$), the dependence on the Reynolds number and distance between the walls has been investigated. In particular, we compared the velocity profiles in wall units for two configurations, with the channel width equal to $2h$ and and $2.2h$ respectively. The velocity profile is obtained by averaging in x, z and time; to determine the origin for y, we followed the approach of Jackson (1981) who determined d_o to be the centroid of the moment of forces acting on the elements:

$$U^+ = 1/\kappa \ln(y - d_o)^+ + C - \Delta U^+ . \qquad (2)$$

The velocity profiles (fig.2 □ and ○) near the rough wall are essentially identical, implying that the precise location of the upper wall is not important. The present results agree with those from Hanjalic & Launder's (1972)experiments at higher Reynolds numbers (between 10.000 and 50.000), i.e. the mean velocity and turbulent intensities, scaled on wall units, do not depend on the roughness on the lower rough wall.

The dependence on the Reynolds number was also investigated by comparing two cases ($w/k = 3$) with the same k^+ and different Reynolds numbers ($Re = 4200$ and $Re = 6000$). For the latter, the number of points in z was increased to 193. Fig. 2 shows that the mean velocity profile in the log-region, and hence the roughness function ΔU^+, do not depend on the Reynolds number but on k^+ only. The flow is therefore in the so-called fully turbulent regime and the present results should be applicable to higher Reynolds numbers. This is consistent with the conclusion of Bandyopadhyay (1987), in the context of this particular surface geometry, that the flow is fully turbulent if $k^+ \geq 20$. In the present simulations, k^+ ranges from about 40 for $w/k = 1$ to about 90 for $w/k = 7$. In figure 2 are also shown the velocity profiles for $w/k = 1, 3, 19$. By increasing w/k the roughness function ΔU^+ increases and is maximum at $w/k = 7$. For $w/k > 7$ it decreases and for very large value of w/k ΔU^+ it is expected to tend to zero. This is in agreement with the experiments by Furuya *et al.* (1976) for rods roughness.

MEAN FLOW

Mean streamlines, averaged with respect to time and z are shown in figure 1. For $w/k \leq 3$, a separation occurs at the trailing edge of the element (point A) and reattachment is on the opposite vertical wall ($\overline{CD}$). The cavity is occupied by a large recirculation zone with two secondary vortices, of opposite direction to the main recirculatory zone, in the corners (D) and (B). The streamlines above the roughness exhibit a weak undulation. For $w/k \geq 7$, the flow reattaches on the bottom wall (point E) at about $5k$ downstream of the back face of the element ($\overline{BE} \simeq 5k$). The near-wall streamlines are essentially horizontal over the region $\overline{EG}$, where $\overline{GD} \simeq 1.5k$. As the next element is approached, the streamlines are tilted upward and separation occurs. This is in close agreement with the flow visualisations of Liu, Kline & Johnston (1966). For $3 < w/k < 7$, the flow structure is intermediate to the previous two. Once w/k exceeds a "critical" value ($\simeq 7$), the flow remains virtually unchanged around a roughness element. The only noticeable difference

in the patterns between $w/k = 7$ and 10 is the length of the region where the streamlines are parallel to the bottom wall ($\overline{EG}$). The size and strength of the recirculation zones do not change for $w/k \geq 7$.

Details of the present simulations such as the pressure and friction on the wall, and the Clauser roughness function may be found in Leonardi 2002. The simulations also focused on the variations of the viscous drag (D_v) and the form drag (D_P) on the ratio w/k. It was observed that, as w/k increased, D_P increased, reaching a maximum for $w/k \approx 8$. On the other hand, D_v decreased to a minimum value for $w/k \approx 6$. Such a behaviour implies that important structural changes occur as w/k varies.

STREAKS AND TWO-POINT CORRELATIONS

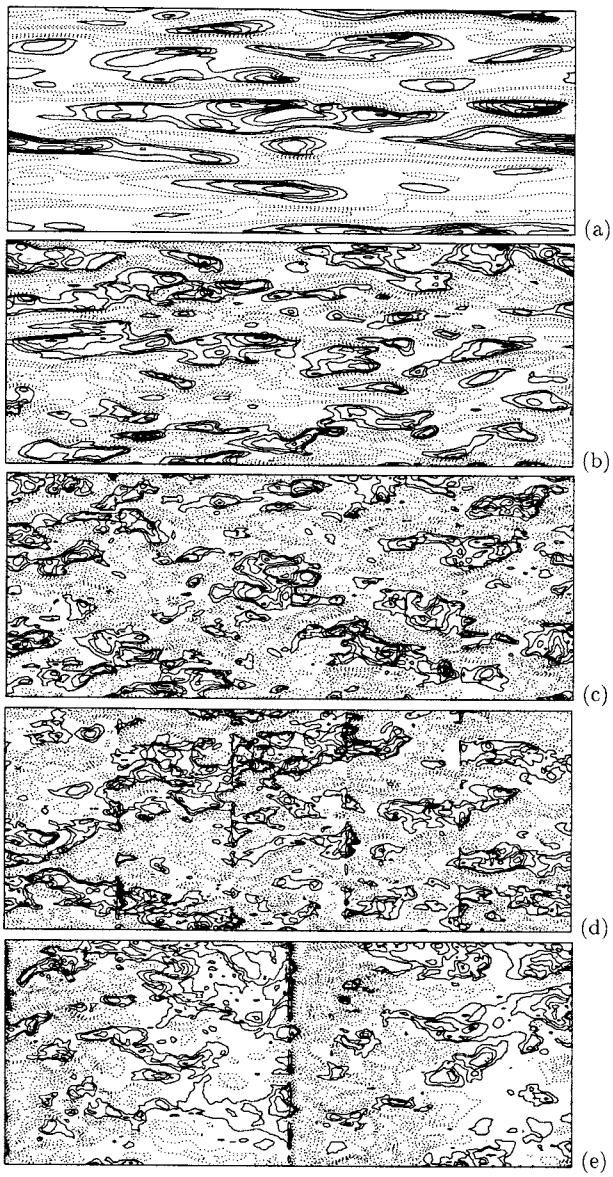

Figure 3: Contour plots of u/u', where a prime denotes an *rms* (———) positive, (·····) negative. (a) Flat channel, (b) $w/k = 1$ (c) $w/k = 3$, (d) $w/k = 7$. Increment .5

The turbulent boundary layer over a flat wall is characterised by elongated streaks which lift up in a pseudo-random manner before breaking down. To assess the effect of the roughness, we compare instantaneous fluctuations of

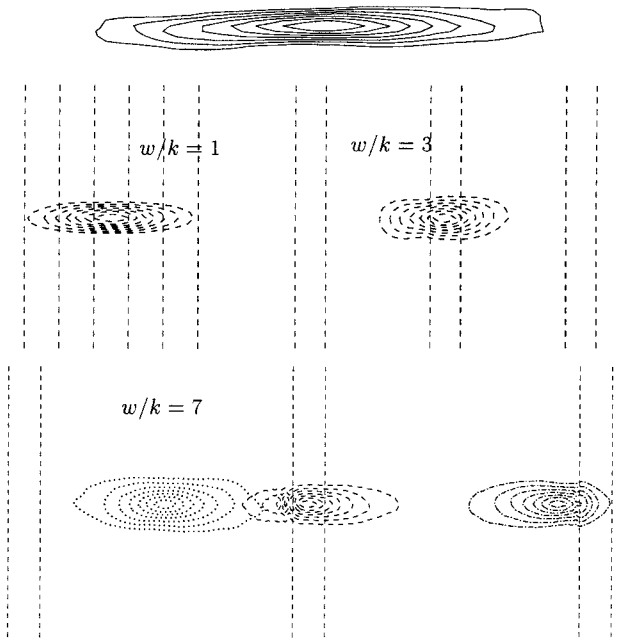

Figure 4: Two-point correlations in the (x,z)-plane $\overline{\rho_{uu}(\mathbf{x_0})}$, $y^+ = 5$. Contour from .3 to 1 (increment is 0.1). Left, $(w/k = 1)$; centre $(w/k = 3)$; right, $(w/k = 7)$. (----), $x = x_a$; (·····), $x = x_b$; (—·—), $x = x_c$. Flow is left to right.

the streamwise velocity (u/u'), (where a prime denotes an *rms*) in horizontal planes (x–z), at $y/h = .03$ (for a flat channel, at this Reynolds number this distance would correspond to $y^+ \simeq 6$). As the velocity fluctuations vary with respect to w/k, to maintain the same increment in all the figures, u was divided by its *rms* value at that y. Elongated structures are found above (fig. 3b) the rough wall with square cavities. These resemble those over the smooth wall (fig.3a) and those revealed in the visualisations of Djenidi *et al.* (1999) for the same surface.

By increasing w/k (figs. 3c,d) fluctuations increase in magnitude. This is due to the increased momentum exchange with the outer layer, as previously observed from a quadrant analysis (Krogstad & Antonia 1992). The width of the structures in z is larger than in the smooth wall case. Very close to the plane of the crest (not shown here), the wall geometry splits the elongated structures into nearly circular regions located above the grooves. The no-slip condition ($u = 0$) on the crests reduces the coherence in the streamwise direction and produces $\partial u/\partial x$. Moreover within the cavity, near the leading edge of the element, $\partial u/\partial x < 0$. Continuity requires $\partial u/\partial x$ to be balanced by $\partial v/\partial y$ and $\partial w/\partial z$ (v and w are the fluctuations of normal and spanwise velocity respectively), thus leading to an enhancement of v and w near the rough wall.

To quantify the previous observations, two-point correlations, with one point fixed, were computed. Figure 4 shows $\overline{\rho_{uu}(x_0)} = \overline{u(x_0)u(x)}/(u'(x_0)u'(x))$ for $w/k = 1, 3, 7$ in horizontal planes (x, z). For reference, the smooth wall contours are included at the top of the figure. A prime denotes an rms value, $\mathbf{x_0} = x_0, y_0, z_0$, are the coordinates of the fixed point, $\mathbf{x} = \mathbf{x_0} + \Delta\mathbf{x}$ is the position of the other point, the overbar indicates averaging with respect to the number of fields and wavelength (i.e. $\overline{u} = \sum_{n,t,z} u(x + n\lambda), t, z)$) Results were obtained at the same y of the previous figures for 3 different x_0: on the crest (x_a, ----), at the centre of the

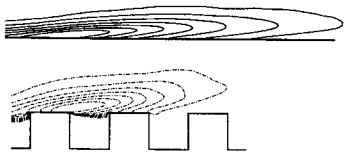

Figure 5: Two-point correlations in the (x,y)-plane $\rho_{uu}(\mathbf{x_0}, 0)$, $y^+ = 6$. Contour from .3 to 1 (increment is 0.1). (top) upper wall (smooth) of the channel, (bottom) $w/k = 1$.

cavity (x_b, ·····), and slightly upstream of a roughness element (x_c, —·—) (see fig. 1). A decreased streamwise coherence, relative to the smooth wall case, is observed for all the rough surfaces. However, even if at $w/k = 1$ contours are considerably less elongated than over the smooth wall, the coherence in x is larger with respect the other surfaces investigated. However it could be surprising that a so small disturbance as square grooves may reduce the streamwise extent of the correlation contours of a factor 2.

This can be explained by analysing $\overline{\rho_{uu}}$ in side sections (x,y). Although the contours remain almost as elongated as over the smooth wall, there is little doubt that their inclination has increased, underlying the increased communication between the cavities and the overlying flow (fig. 5). The increased inclination is also consistent with the reduced streamwise correlation over this surface in figure 4.

By increasing w/k, the spanwise extent of the structures increases and the streamwise length decreases. For $w/k = 1$, 3 there is only a weak dependence on the location of x_0, whereas for $w/k = 7$, the correlation contours are less elongated near or over the roughness element crest than within the cavity.

The decreased coherence in the streamwise direction is due to normal wall motion induced by the roughness. To show how the velocity field is perturbed by the square bars on the bottom wall, instantaneous isosurfaces of ω_y ($\equiv \partial u/\partial z - \partial w/\partial x$) were computed (fig. 6). For $w/k = 1$, the contours are parallel to the plane of the crests and very similar to those over a flat wall although shorter. For this geometrical configuration, the influence of the rough surface on the overlying flow is small and in fact this is the case for which ΔU^+ is smallest and the streamwise correlation of u is most similar to that on a flat wall. While for $w/k = 1$ positive and negative contours alternate regularly in z as over a flat wall, for $w/k = 7$ the vorticity field is more complex. The fluctuations of v and w, due to the "splashing" effect occurring near the leading edge of an element, lift the structures upward and increase their width in z. Upstream the element, a negative (dark) contour of ω_y almost normal to the wall can be observed.

The correlation in the spanwise direction, $R_{u,u}(r,y) = \overline{u(x,y,z)u(x,y,z+r,t)}$ further corroborate the loss of alternating structures of positive and negative sign for $w/k = 7$ (fig.7). While for $w/k = 1$, $R_{u,u}$ has a minimum at about $z^+ = 50$, similar to the smooth wall case, for larger values of w/k, $R_{u,u}$ gradually decreases in z without a defined minimum. The extent of the correlation in z increases by increasing w/k and has a maximum for $w/k = 7$.

To quantify the outward motion due to the roughness, the correlation $\langle \rho_{vv}(x_0) \rangle = \langle v(x_0)v(x) \rangle / (v'(x_0)v'(x))$ was computed. Angular brackets indicate averaging with respect to z, the number of fields and wavelength. Figure 11 shows $\langle \rho_{vv}(x_0) \rangle$ for $w/k = 1, 3, 7, 19$ in vertical planes (x, y) compared with the smooth wall.

For a flat wall, the contours of ρ_{vv} are elongated in x. In

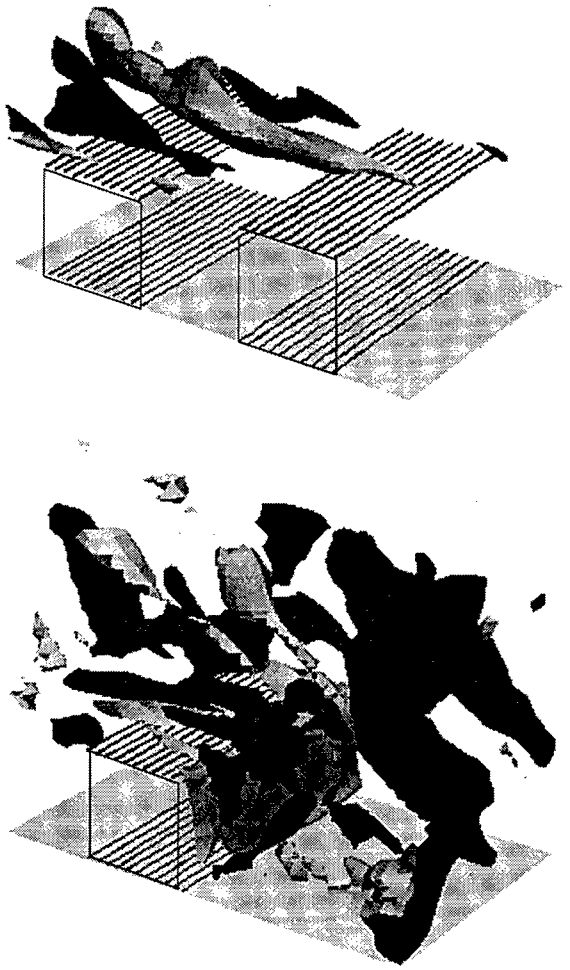

Figure 6: Contours of instantaneous ω_y. Top: $w/k = 1$, bottom: $w/k = 7$ Flow is right to left. Dark $\omega_y = -4$, light $\omega_y = 4$.

fact the streaks gradually lift-up, oscillate and finally break down, so that there is a relatively wide region in x over which the normal velocity is correlated. The case $w/k = 1$ is similar to the smooth wall even if the contours are less elongated. Hence, as for the u contours, there is quite a close similarity between the flat wall and a rough wall with $w/k = 1$. By increasing w/k, the contours depart from those over a flat surface, and for $x = x_b$ and $x = x_c$ the correlation in y is even larger than in x. In particular, near the leading edge, the correlation in y is largest, and we expect that this is the region where the flow is more likely to be ejected out of the cavity (this is further corroborated by a quadrant analysis not shown here, see Leonardi 2002). No significant differences are observed at $x = x_a, x_c$ for $w/k = 19$ and $w/k = 7$. For $w/k \geq 7$, the elements can be considered as 'isolated'. As for $w/k \geq 7$, separation occurs over the crests (Leonardi 2002), the correlation contours (at $x = x_a$) closely resembling the recirculation region over the crest.

TURBULENT INTENSITIES AND ANISOTROPY INVARIANTS

The intensity of the outflows near the rough wall can be assessed by comparing the present *rms* distributions with those of Kim *et al.* (1987) (fig.9). Here, only the portion

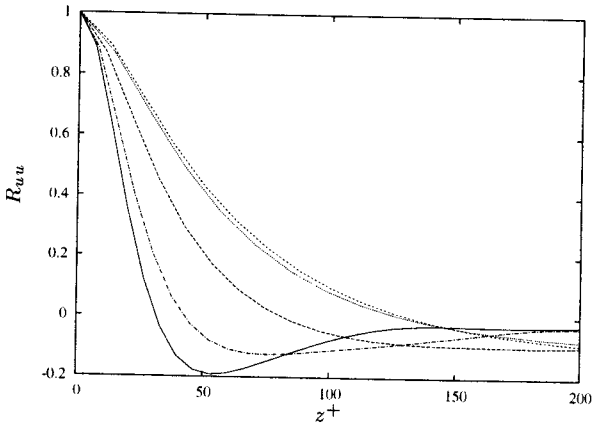

Figure 7: Two-point correlation coefficients at $y^+ \simeq 10$ in spanwise direction. Symbols as in fig.2.

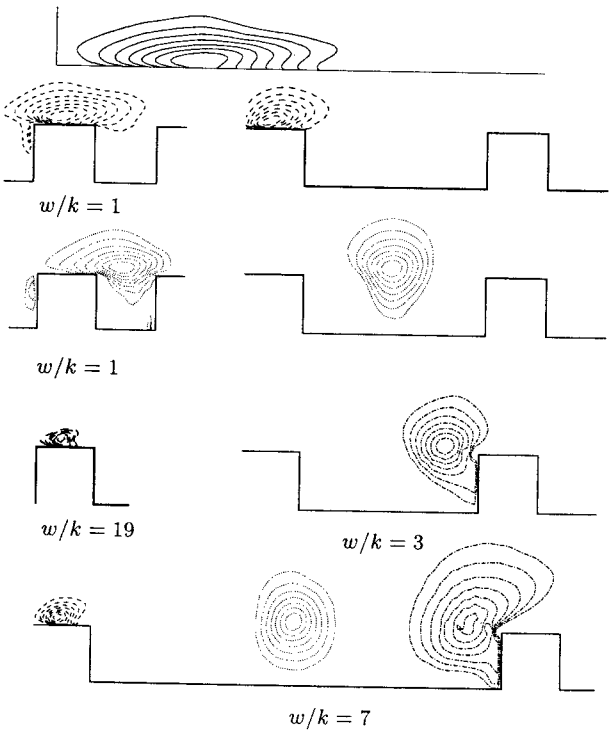

Figure 8: Two-point correlations in the (x,y)-plane $\langle \rho_{vv}(\mathbf{x_0}) \rangle$, $\tilde{y}^+ = 6$. Contour levels range from .3 to 1 (increment is 0.1). Top, flat wall (———). (----), $x = x_a$; (·····), $x = x_b$; (—·—), $x = x_c$. Flow is left to right.

above the plane of the crest is shown, and averaging was also performed over x. Near the wall, $\langle u^{+2} \rangle$ is largely reduced despite an increase in $\langle u^2 \rangle$. As expected, $\langle v^{+2} \rangle$ is larger than over a flat wall, with the maximum very close to $y = 0$. A corresponding increase is found in $\langle w^{+2} \rangle$. As noted earlier, v and w are enhanced near the rough wall, as a result of continuity.

For $w/k = 3$ and $y/h \geq .45$, $\langle u^{+2} \rangle$ and $\langle w^{+2} \rangle$ closely overlap those obtained by Kim *et al.* (1987) while $\langle v^{+2} \rangle$ is larger than that over a flat wall up to $y/h = .8$. Hence, for this particular configuration, the influence of the rough surface is confined up to about 4 roughness heights.

For $w/k = 7$, both $\langle u^{+2} \rangle$ and $\langle v^{+2} \rangle$ remain bigger than those by Kim *et al.* for a large layer above the wall. In fact $\langle v^{+2} \rangle$ coincides with the value of Kim *et al.* only at $y/h = 1$. (5 roughness heights above the wall) and $\langle u^{+2} \rangle$ present a

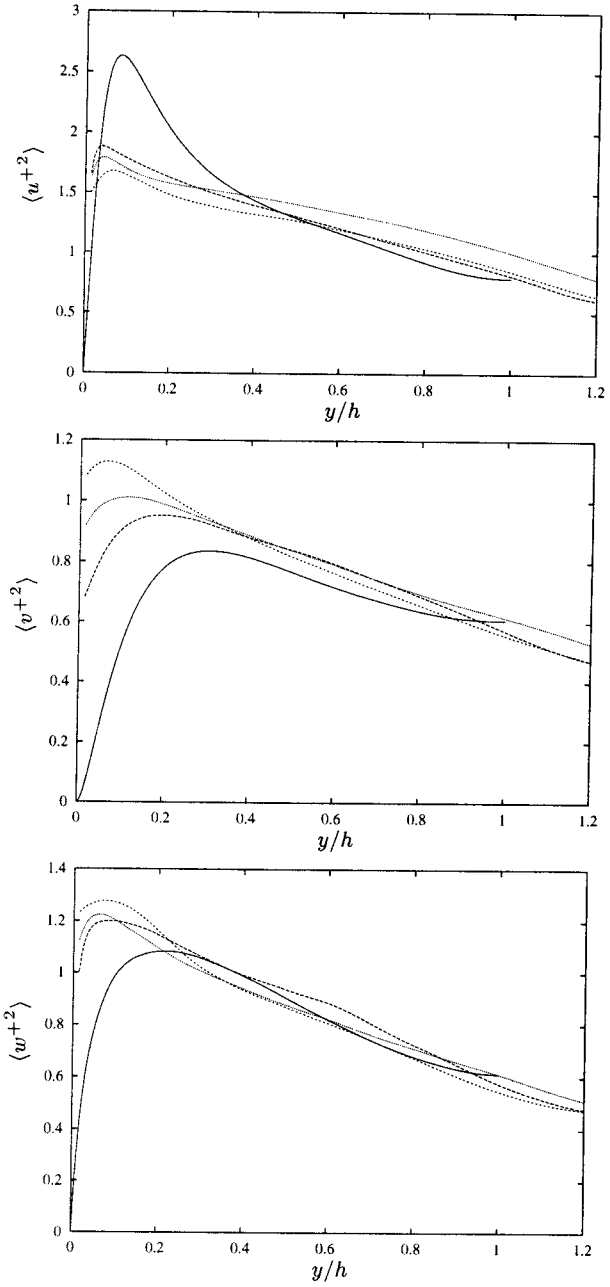

Figure 9: Turbulent intensities averaged in time x and z. ——— Kim *et al.* (1987) ---- $w/k = 3$, ····· $w/k = 7$, ---- $w/k = 19$.

different (smaller) slope and overlap the curve relative to the flat channel at $y/h = 1.4$ (7 roughness heights above the wall).

For $w/k = 3, 7, 19$, $\langle v^{+2} \rangle$ and $\langle w^{+2} \rangle$ coincide for $y/h >$ .4, and being $\langle u^{+2} \rangle$ greater than the other two the turbulence is the so called 'cigar-shaped' turbulence.

An estimate of the overall anisotropy is in the Reynolds stress anisotropy tensor $b_{ij} = \langle u_i u_j \rangle / \langle u_i u_i \rangle - \delta_{ij}/3$ (Lumley 1978). Here, $\langle u_i u_i \rangle$ is twice the turbulent kinetic energy (TKE), (where $u_1, u_2, u_3 \equiv u, v, w$), and repeated index summation is implied. δ_{ij} is the Kronecker delta function. A convenient method for comparing the overall anisotropy is given by the function $F = 1 + 9\text{II} + 27\text{III}$, where II[$\equiv -b_{ij}b_{ji}/2$] and III[$\equiv b_{ij}b_{jk}b_{ki}/3$] are the second and third invariants of the tensor b_{ij}. The function F is

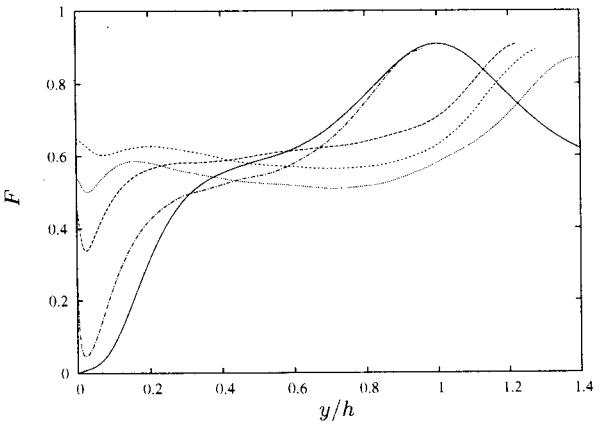

Figure 10: Invariant $F = 1 + 9II + 27III$ for square bars roughness: symbols as in figure 2

a measure of the approach to either two-component turbulence ($F = 0$) or a three-component isotropic state ($F = 1$). In a flat channel, isotropy is quite poor near the walls, due to the organisation associated with the quasi-longitudinal structures, and best at the centreline. As the three stresses do not coincide, F is smaller than 1. Figure 10 shows that near the roughness and within the cavities, the isotropy is definitely increased, and the maximum is shifted beyond the centreline. For large values of w/k, a region of constant F extends over about $3k$. A comparison of F at the same y for $y > 3k$ could lead to the conclusion expressed by Mazouz *et al.* (1998)(and in disagreement with what is generally found in the literature)that roughness increases the anisotropy. At the centreline of $w/k = 7$, the difference between $\langle u^{+2} \rangle$ and $\langle v^{+2} \rangle$, $\langle w^{+2} \rangle$ is larger than for a smooth channel. This is due to the upward shift produced by the roughness, and not to a genuine decrease in isotropy, the peak having about the same intensity and occurring at about $y/k = .5$. The case $w/k = 1$ is, as expected from the previous figures, closest to the flat wall.

CONCLUSIONS

The present direct numerical simulations indicate that structures near a rough wall are less elongated than over a smooth wall. By increasing w/k, the coherence in x is reduced while it is increased in z. The changes in the structures may be related to the strength of outward ejections of fluid from the cavities;this strength reaches its maximum for $w/k = 7$. The increased intensity of the wall-normal velocity fluctuations is coupled to an increased strength in the spanwise velocity fluctuations, which is difficult to measure reliably in experiments. On the other hand, the streamwise velocity fluctuation is not very different to that on a smooth wall. Hence isotropy, close to the wall, is better approximated over a rough than a smooth wall. The dependence on w/k is very strong; for very small values of w/k, structures and turbulent intensities resemble those over a flat wall. For $w/k = 3$, the effect of the wall extends up to about $2k$ above the plane of the crests, while for $w/k = 7$, the distance is as large as $5k$. The ratio $w/k = 7$ is that for which with the roughness function ΔU^+ is largest(Leonardi 2002).

ACKNOWLEDGEMENTS

LD and RAA are grateful to the support provided by the Australian Research Council. This research has been supported by MURST 60 %. Discussions with P.-Å Krogstad were appreciated. E. Mostarda is acknowledged for having provided some of his results.

REFERENCES

Bandyopadhyay, P.R. (1987). "Rough-wall turbulent boundary layers in the transition regime". *J.* Fluid Mech. **180**, pp.231–266.

Cantwell B.J. (1981), "Organized motion in turbulent flow" *A*nn. Rev. Fluid Mech. **13**, 457–515

Djenidi, L., Elavarasan, R. and Antonia, R.A. (1999). " The turbulent boundary layer over transverse square cavities". *J.*Fluid Mech. **395**, 271–294.

Fadlun E.A., Verzicco, R., Orlandi P. and Mohd-Yusof, J. (2000). " Combined immersed boundary finite-difference methods for three-dimensional complex flow simulations". *J.* Comput. Phys. **161**, 35–60.

Furuya, Y., Miyata, M. & Fujita, H. (1976). "Turbulent boundary layer and flow resistance on plates roughened by wires". *J.* Fluids Eng. **98**, 635–644.

Grass, A.J., Stuart, R.J., Mansour-Thehrani, M. (1993). " Common vortical structure of turbulent flows over smooth and rough boundaries". *A*IAA J. **31** , 837–846.

Hanjalic & Launder (1972). "Fully developed asymmetric flow in plane channel". *J.* Fluid Mech. **51**, 301–335.

Jackson, P.S. (1981). "On the displacement height in the logarithmic profile". *J.* Fluid Mech. **111**, 15–25.

Kim J., Moin, P. & Moser, R. (1987) "Turbulence statistics in fully developed channel flow at low Reynolds number". *J.*Fluid Mech. **177**, 133–166.

Kline, S.J., Reynolds, W.C., Schraub, F.A. and Runstadler, P.W. (1967). "The Structure of Turbulent Boundary Layers". *J.*Fluid Mech. **30** , 741–773

Krogstad,P.-Å and Antonia, R.A. (1992) "Comparison between rough- and smooth-wall turbulent boundary layers. *J.*Fluid Mech. **245**, 599–617.

Krogstad, P.-Å and Antonia, R. A. (1994). " Structure of turbulent boundary layers on smooth and rough walls". *J.*Fluid Mech. **277**, 1–21.

Leonardi (2002) "Turbulent channel flow with roughness: Direct Numerical Simulations". PhD Thesis University of Rome "La Sapienza".

Liu, C.K., Kline, S.J. and Johnston, J.P. (1966). "An experimental study of turbulent boundary layers on rough walls". Report MD-15, Department of Mechanical Engineering, Stanford University.

Lumley J.L. (1978) "Computational modeling of turbulent flows". *A*dv. Appl. Mech. 18: 123–176.

Mazouz A., Labraga L. & Tournier C. (1998) "Anisotropy Invariants of Reynolds Stress Tensor in a Duct Flow and Turbulent Boundary Layer". *J.* of Fluid Eng. **120**, 280–284.

Orlandi, P. (2000) "Fluid Flow Phenomena : A Numerical Toolkit" *D*ordrecht, Kluwer.

Perry, A. E., Schofield, W. H. and Joubert, P. N. (1969) "Rough wall turbulent boundary layers". *J.* Fluid Mech. **37**, 383–413.

Robinson S. K., (1991) "Coherent motions in the turbulent boundary layer" *A*nn. Rev. Fluid Mech. pp. 601-639.

Wood D.H. and Antonia R.A. (1975) "Measurements of a turbulent boundary layer over a d-type surface roughness". *J.* Appl. Mech. **42** 591–597.